1   *Geophysical Research Letters*

2   Supporting Information for

3   **Slow dynamics of hydrate systems revealed by a double BSR**

4   M. Fabre[1, 2]*, V. Riboulot[1], L. Loncke[2], S. Ker[1], G. Ballas[3], Y. Thomas[1], G. Ion[4], N. Sultan[1]

5   [1] Geo-Ocean, Université de Brest, CNRS, Ifremer, Plouzané, France

6   [2] CEFREM, Université de Perpignan Via Domitia, France

7   [3] Geosciences Montpellier, Université de Montpellier, CNRS, France

8   [4] GeoEcoMar, Bucharest, Romania

9

Contents of this file

Introduction

This Supporting Information supplied with the manuscript includes:

- the acquisition and processing parameters of the presented high-resolution seismic section (**Text S1 and Fig. S1**);
- the modelling method and inputs (**Text S2 and Figs. S2, S3, S4, S5**);
- the table of tested scenarios (**Text S3 and Table S1**);
- the detailed of modelling results (**Figs. S6 and S7**).

Text S1: Acquisition and processing parameters of the presented seismic section

High-Resolution Seismic Data

The 2D High-Resolution (HR) seismic profile *33c* used for this study was acquired during GHASS-cruise (GHASS cruise (2015); https//doi.org/10.17600/15000500) using a 96-channel streamer of 6.25-m trace spacing and a maximum source-receiver offset of 650 m (Fig. S1A). The seismic source consisted of a single small air gun (24 cubic inches) deployed at 1.5 m whereas the streamer was towed at a depth of 2 m to optimise resolution. The resulting source signature has a 40–170 Hz frequency bandwidth with a central frequency of 110 Hz. Profile *33c* was processed using a poststack sequence (Ker et al., 2019). HR velocity analyses were performed on super gathers every 150 m corresponding to the lateral resolution of the resulting velocity field. The picking of RMS velocities was performed on semblance panels using a horizon-consistent approach. Interval velocities were computed using Dix approximation. The 2D velocity model was then used to perform the post-stack depth Kirchhoff migration.

Very High-Resolution Deep-Towed Seismic Data

Very High-Resolution (VHR) deep-towed multichannel seismic data was also acquired during the GHASS cruise with Ifremer seismic equipment (SYstème SIsmique de Fond, SYSIF). SYSIF is composed of a Janus-Helmholtz acoustic source (220-1050 Hz) and a 52-channel streamer with a maximum offset of 110 m, tailored for working under high- hydrostatic pressure environments (Ker et al., 2010; Marsset et al., 2014). Seismic resolution of the SYSIF profile PL01PR03 presented in Figure S1B is less than 1 m vertically and 3 m horizontally.

Text S2. Modelling Method

To constrain the range of variability of paleo-gas hydrate stability zones, which have evolved since the LGP (Last Glacial Period), we ran a 2D transient heat equation model with the temperature and pressure of hydrate-phase equilibrium calculated at each time step using the van der Waals and Platteeuw model (Sultan et al., 2010). We implemented the approach by considering major environmental changes in the Black Sea Basin. This was achieved using initial, limit, and boundary conditions obtained from direct in-situ measurements such as porosity, thermal diffusivity (Riedel et al., 2020), gas composition (99.6% pure methane and the remaining 0.4% mainly N_2, from Riboulot et al., 2018), partly acquired during the GHASS cruise (2015). In addition, we have considered various scenarios that take into account indirect assessments of factors and properties evolving over time, such as sea-bottom temperature, thermal conductivity, salinity, sea-level variations, and seafloor morphology, which were integrated into the calculation. Further details regarding these scenarios are reported in Figures S2, S3 and S4. The seafloor morphology evolution through time provided from the seismic line is presented in Figure. S5.

The thermal field was calculated by defining the maximum depth of thermal perturbation caused by a change in seawater temperature, using the method developed by Goto et al., (2005). Considering a temperature disturbance over a period of 10,000 years and a mean thermal diffusivity of 3.10^{-7} m²/s (Riedel et al., 2020), we determined that the depth of the perturbation corresponds to 758 m. In this method, a constant temperature was imposed at the base of the calculation, resulting in a change in the thermal gradient with time (Fig.

66   S3). It is important to emphasise that this change is not related to a variation in the deep

67   thermal flux but rather to the perturbation of seawater temperature.

68   **Text S3. Tested Scenarios**

69   Since the objective of the study was to simulate the position of the Gas Hydrate

70   Stability Zone (GHSZ), in comparison with the geophysical observation of the second

71   BSR, we conducted numerical calculations for five different scenarios (Table S1). The

72   results of the two scenarios (cases A and D) considering sea level amplitude variations

73   between -15.7 and -9 ka (Fig.S2A) did not yield any significant differences in the

74   modelling results (Fig. S6). However, the modelling results revealed a pronounced

75   sensitivity of GH dynamics to the different sea-bottom temperature scenarios proposed by

76   Erickson and Von Herzen, (1978) and Zander et al., (2017) for the last 9,000-yr period

77   (Fig. S2B); These scenarios mainly differed by the delay of temperature re-equilibrium

78   which occurred following the connection with the Mediterranean, leading to a varied

79   progression of the GHSZ seaward towards its present day location (see modelling results

80   between -9 to 0 ka presented in *Cases A, B* and *C* in Fig. S6). Therefore, to complete the

81   parametric study, we conducted a series of additional scenarios by varying the sea-bottom

82   temperature at LGP (including values of 3°C and then 3.5°C, in addition to the initial value

83   of 4°C provided from in-situ measurements). We show that even slight variations in sea-

84   bottom temperature have a significant impact on the final results (Fig. S7). Lastly, the

85   hypothesis of a thermal gradient of 30.4°C/km at -9 ka, calculated from MeBo200

86   measurements of 23.8°C/km (Fig. S3), reveals that the calculated positions of the predicted

87   Base of GHSZ (BGHSZ) at LGP and present-day are highly correlated with the position

88   of observed BSR1 and BSR2. A synthesis of the modelling results in the form of four

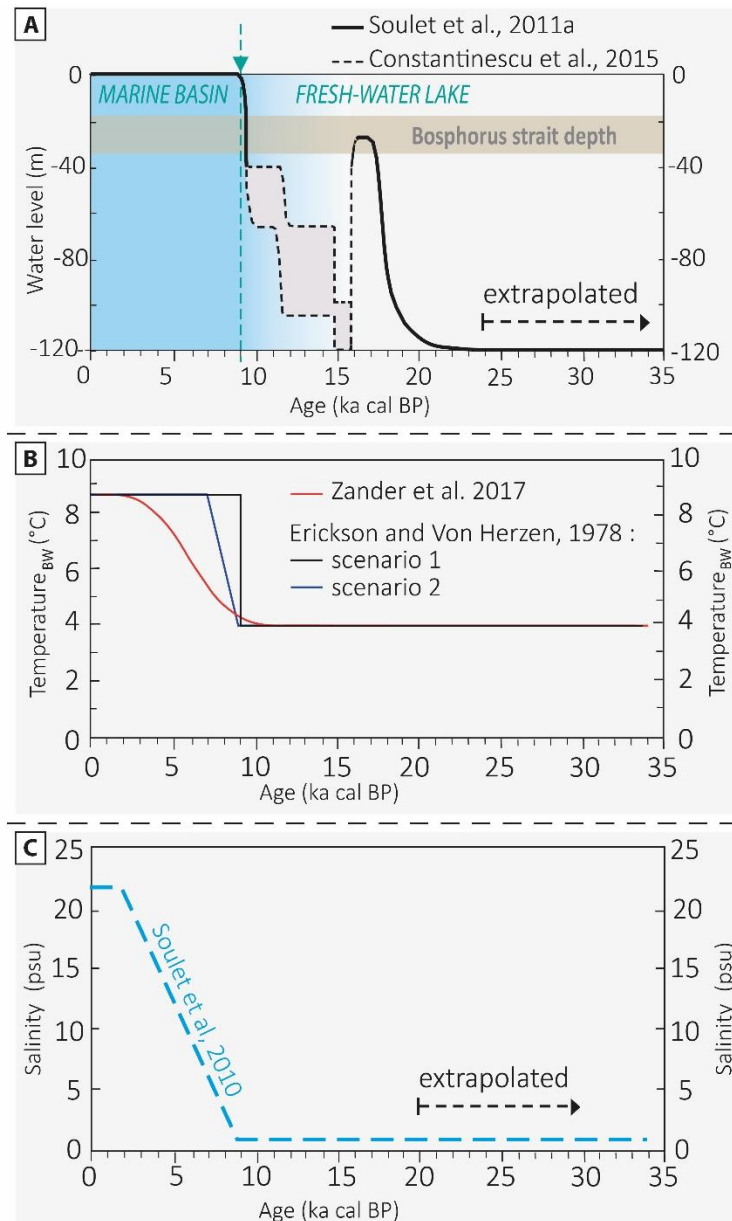89   envelopes is shown in Figure 2B for different ranges of time.

90
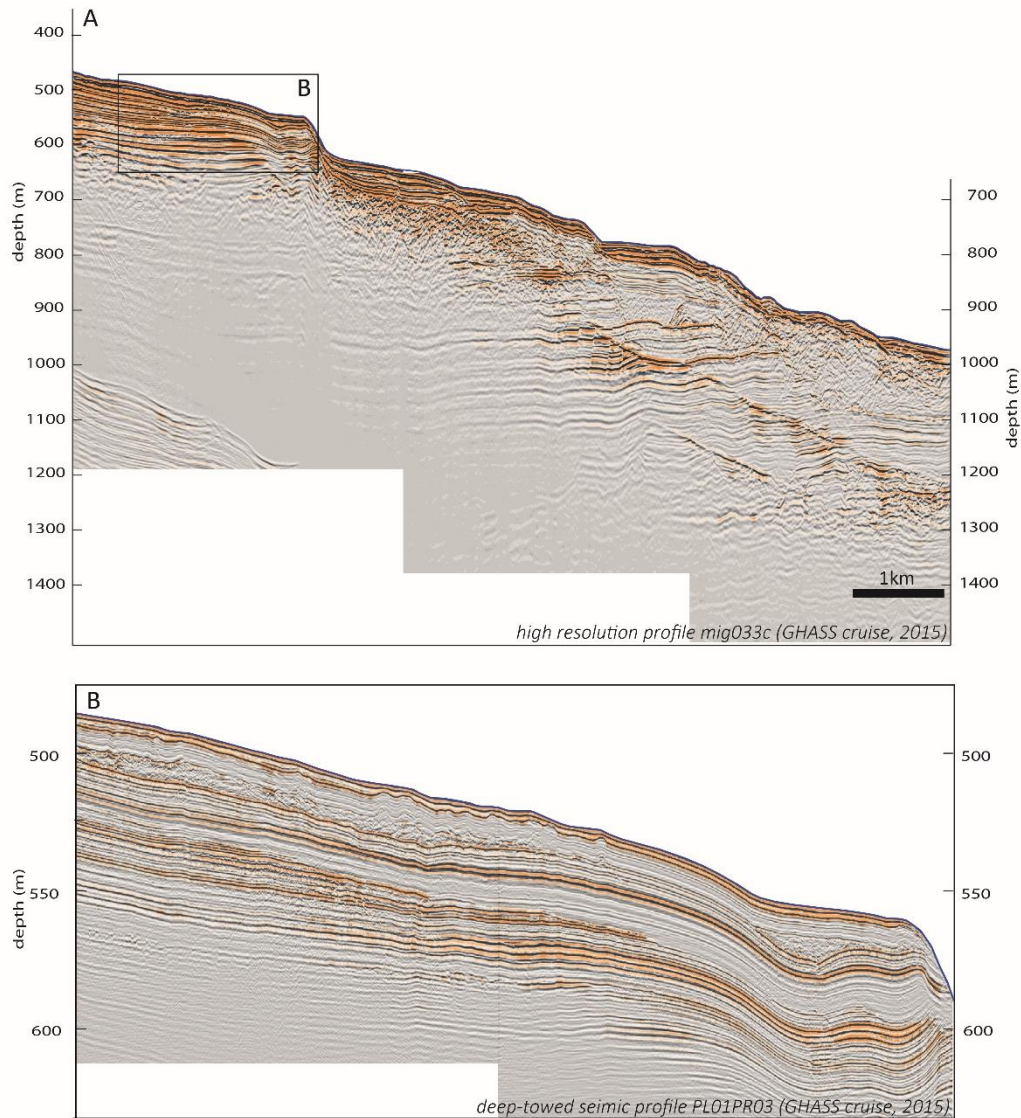
91

92   **Figure S1.** (A) HR seismic profile 33c used for the present study. (B) Deep-towed seismic

93   profile PL01PR03 used to show the landward termination of the second BSR presented in

94   Figure 2, inset d. Locations of the profiles are presented on the Figure 1.

95

96

Figure S2. Modelling inputs: (A) Sea level fluctuations: Two sea-level curves are proposed
by Soulet et al., (2011, 2013) and Constantinescu et al., (2015) on the basis of turbidite
activity in the Danube canyon, and contemporary slightly differing meteoric water runoff:
Scenario 1 is the "lowest sea-level amplitude scenario" between -15,700 ± 300 cal a. BP
and - 9000 cal a. BP, Scenario 2 is the "highest sea-level amplitude scenario" between -
15,700 ± 300 cal a. BP and - 9000 cal a. BP, (B) The sea-bottom temperature was derived

103 from recent in-situ measurements acquired during the GHASS cruise (2015) (Riboulot et

104 al., 2017) for current environmental conditions, considering a fixed temperature of 8.9°C.

105 A sea-bottom temperature of ~4°C was determined for the LGP by Soulet et al., (2010): 3

106 scenarios have been published differing on the timing of sea bottom water warming after

107 the re-connection between the Black Sea and the Mediterranean at 9,000 cal a. BP:

108 Scenario 1 corresponds to the most abrupt temperature change proposed by Erickson and

109 Von Herzen, (1978), Scenario 2 corresponds to a less abrupt temperature change with a 2

110 ka time lapse considered for reaching current temperatures published by Erickson and Von

111 Herzen, (1978), Scenario 3 corresponds to a more progressive sea-bottom temperature re-

112 equilibrium proposed by Zander et al., (2017), (C) The water column salinity was derived

113 from the measured of chloride profile over 25 mbsf for the current salinity (Riboulot et al.,

114 2018). Related to the salt diffusion in sediments occurring progressively since Black Sea

115 and Mediterranean reconnection at 9,000 cal a. BP (Hillman et al., 2018; Riedel et al.,

116 2020), we assume a gradual fall in salinity from 21.9 psu (Practical Salinity Unit) at the

117 seafloor level during LGP (Soulet et al., 2010) to near 2 psu from -2,500 cal a. BP at around

118 28 mbsf.

119
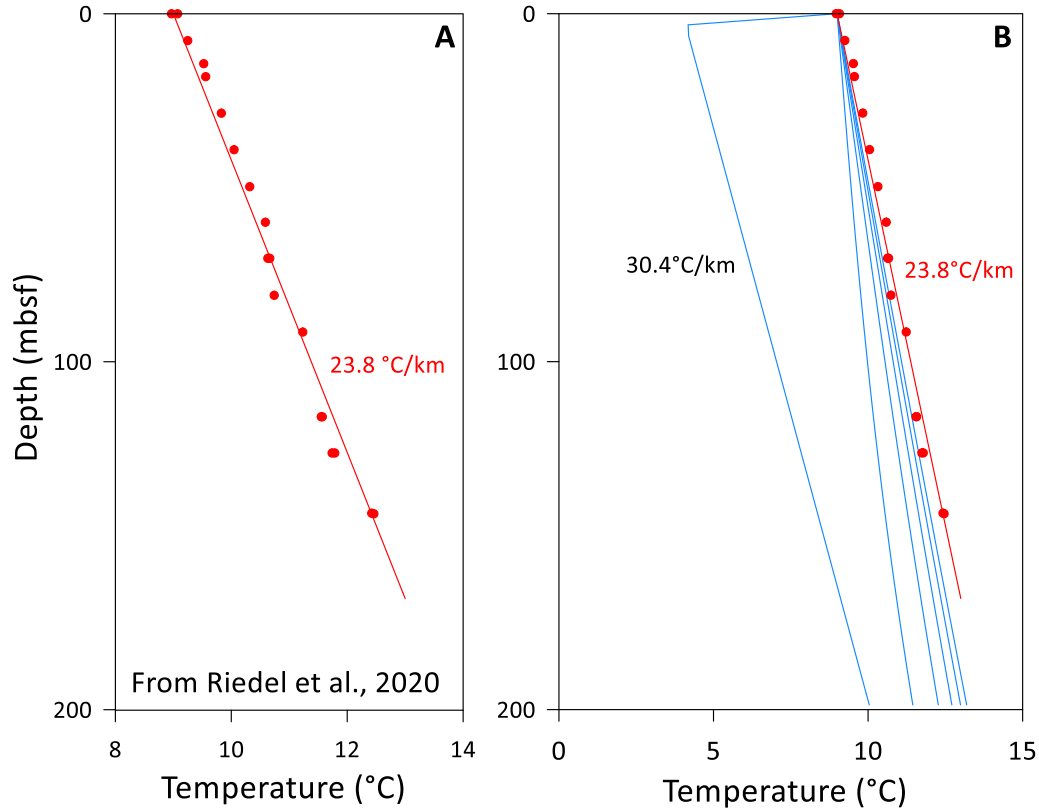
Figure S3. (A) The present thermal gradient of 23.8°C/km was derived from the 150 m long MARUM-MeBo200 seafloor drilling data collected during SUGAR-III project in the study zone (Riedel et al., 2020); (B) Thermal gradient before 9,000 cal a BP, is derived from the thermal diffusivity and porosity inferred from Riedel et al., (2020) presented in Figure S4 and by considering constant temperature at the base of the calculation at 758 mbsf (from Goto et al., 2005 method).

128
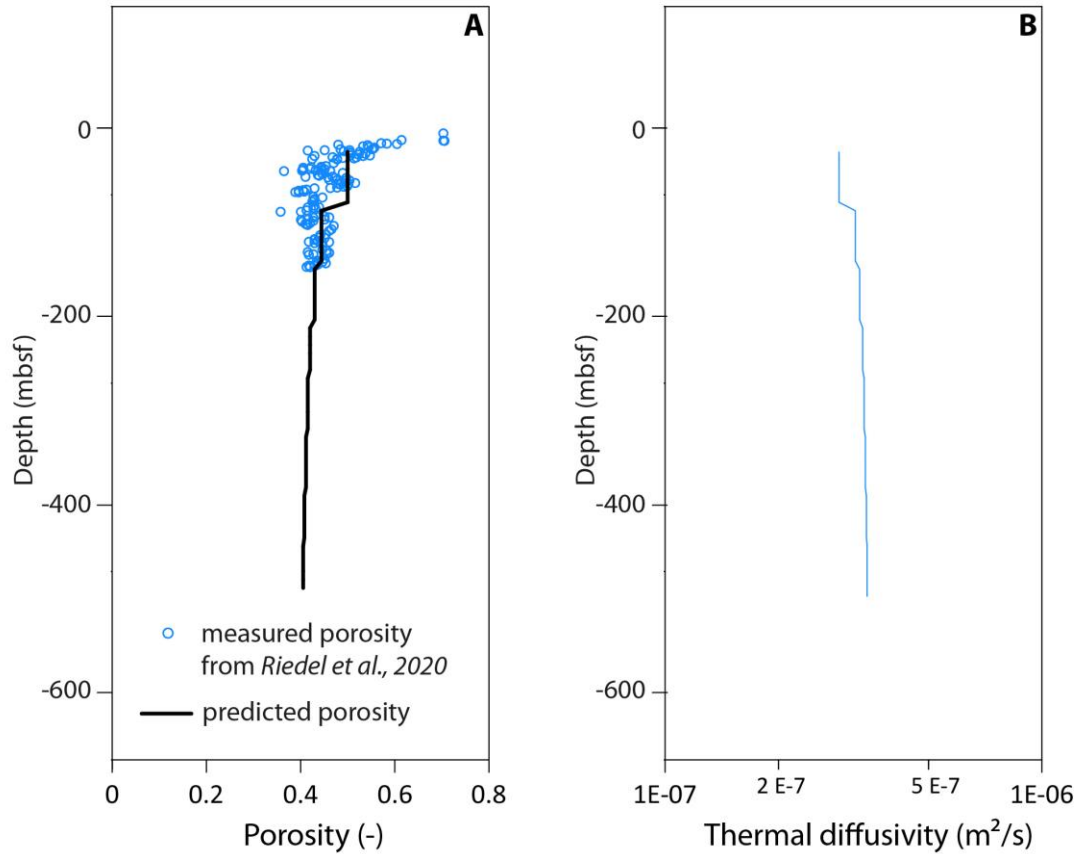
Figure S4. Initial porosity and thermal diffusivity of the sediments as a function of depth

used for the thermal gradient estimation at past conditions (Figure S3). (A) Porosity values

provided from the 150 m long MARUM-MeBo200 seafloor drilling data collected during

SUGAR-III project (Riedel et al., 2020) (blue circles). Based on the porosity law

established from measurements on the first 150 m below seafloor, the porosity pattern has

been predicted down to depths of over 1000 meters for the present study (black bold line);

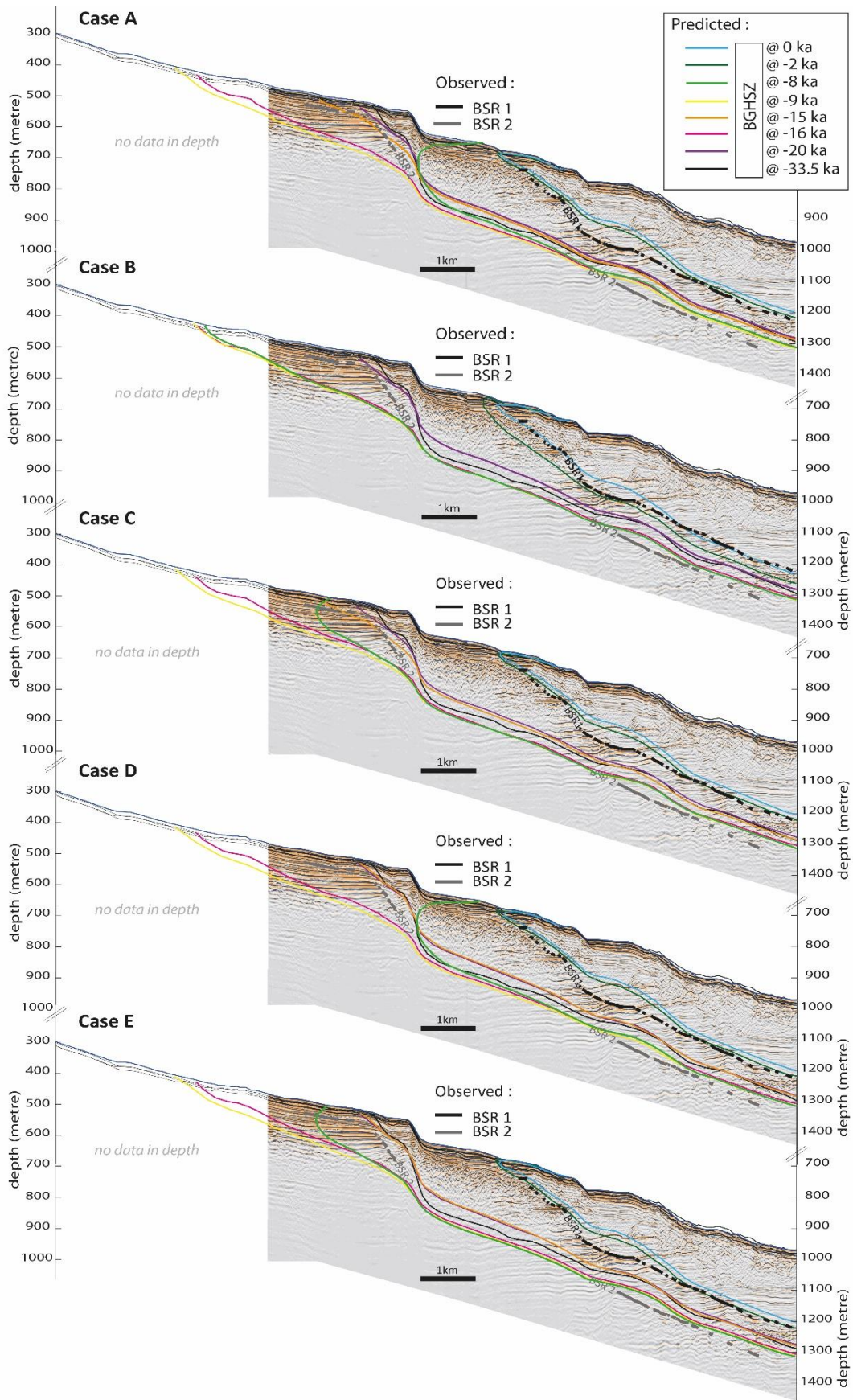(B) The thermal diffusivity of the sediments is derived from porosity.

136
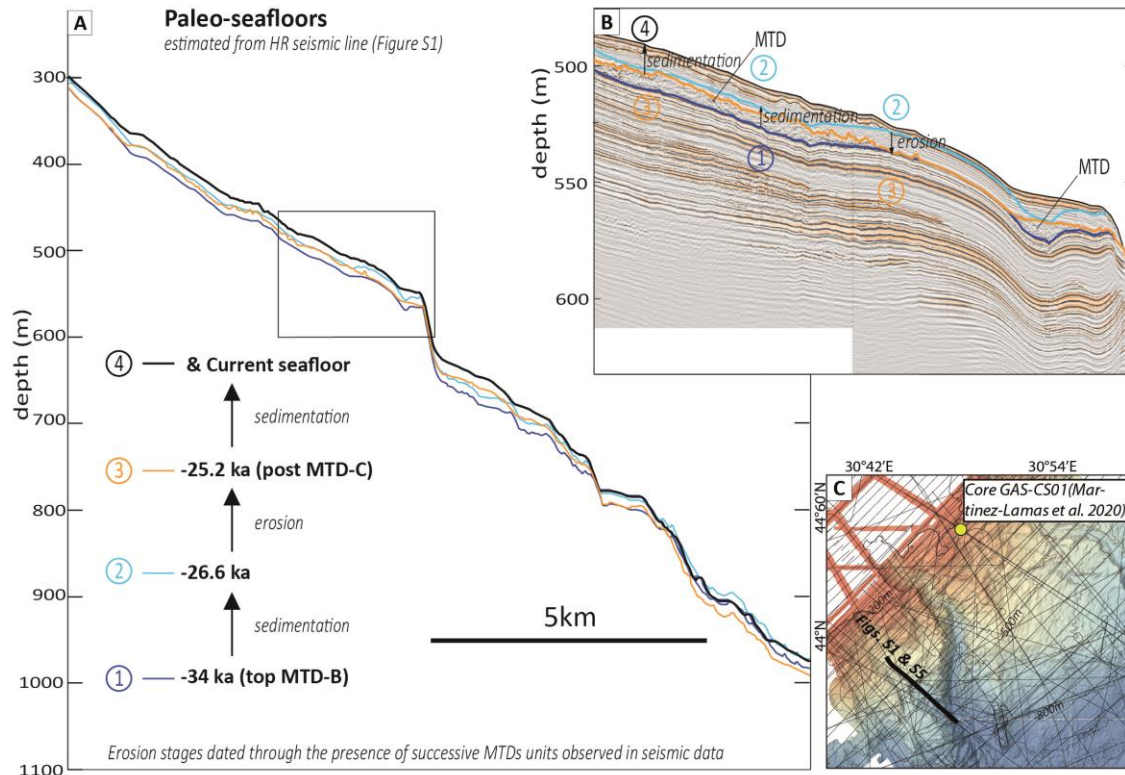
Figure S5. (A) Definition of the different paleo-seafloors used for modelling. Paleo-seafloors are directly extracted from the reference seismic line presented in Figure S1. The ages of successive paleo-seafloors come from dating published by Martinez-Lamas et al. (2020) on a core GAS-CS01, collected 12 km north, at 240 m water depth (yellow dot in C), after the different reflectors have been propagated through numerous sub-bottom profilers (thin black lines in C) acquired during the GHASS and GHASS-2 cruises. The oldest paleo-seafloor 1 (dark blue line in B) dated to -33.5 ka, corresponds to the last lowstand stage time line (LGP) defined by Martinez-Lamas et al., (2020).Paleo-seafloors 2, dated to -26.6 ka and located above the paleo-seafloor 1 (dark blue line in B), results in the seafloor equilibrium after a sedimentation stage (light blue line in B). It is calculated considering a local sedimentation rate derived from the thickness of sediment between corresponding reflectors, in a zone without sedimentary hiatus. Paleo-seafloors 3, dated to

150   -25.2 ka, can be considered as precise accurate time lines after an erosive process (yellow

151   line in B).

152

Case A

Case B

Case C

Case D

Case E

Predicted :
@ 0 ka
@ -2 ka
@ -8 ka
@ -9 ka
@ -15 ka
@ -16 ka
@ -20 ka
@ -33.5 ka
BGHSZ

Observed :
BSR 1
BSR 2

no data in depth

153

12

154 **Figure S6.** Modelling results for the different cases presented in Table S1 have been

155 superimposed over the HR seismic line located in the study zone, along the upper slope of

156 the western Black Sea margin (Fig. 1). Each predicted coloured line represents the

157 distribution of the BGHSZ position computed at different times (-33.5ka; -20ka, -16ka, -

158 15ka, -9ka, -8ka, -2ka, 0ka) since the LGP. To facilitate the comparison between predicted

159 BGHSZ and geophysical observations, BSRs have been highlighted by a black bold line

160 for the current one (BSR1) and a grey bold line for the deeper one (BSR2). Paleo-seafloor

161 inputs on the modelling (Figure S5) have been plotted in black.

162

163

164
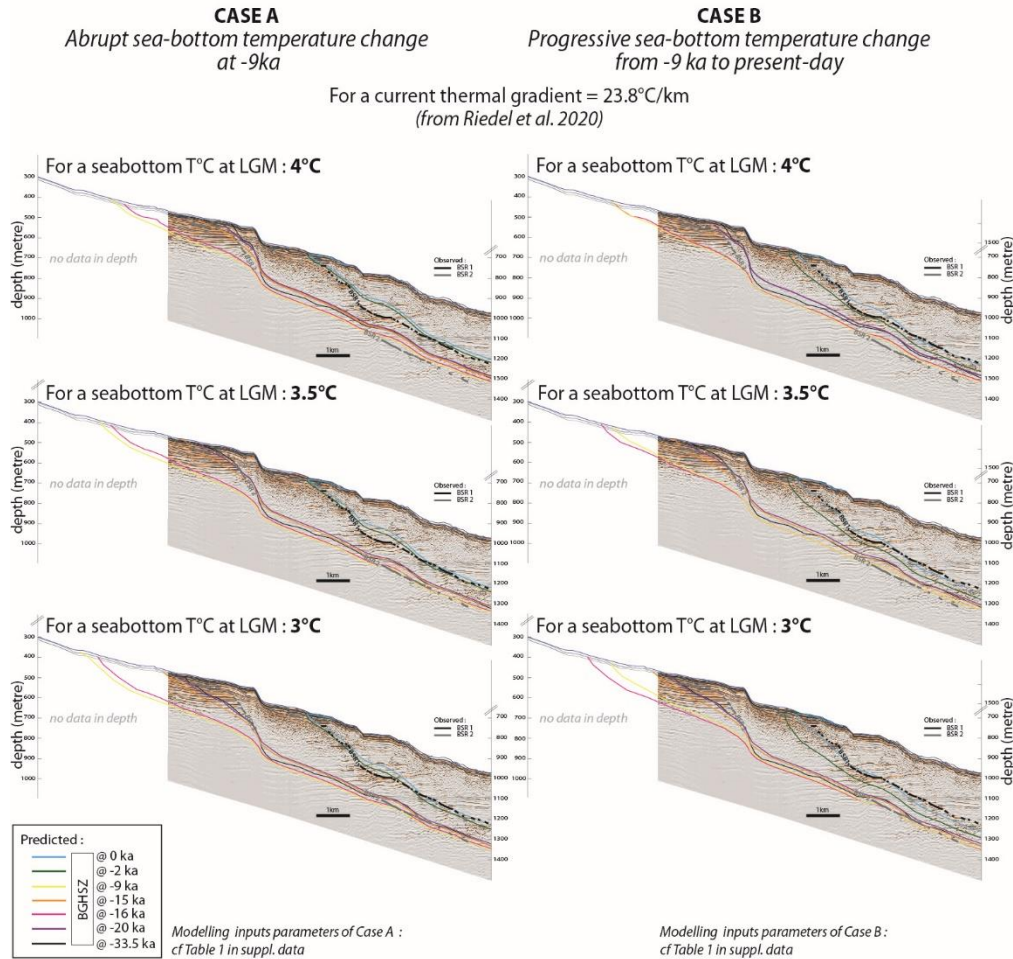
Figure S7. Sea-bottom temperature variations tested for cases A and B –The Predicted
BGHSZ have been redrawn on reference HR seismic line. These two cases consider the
lowest amplitude sea-level variations between 16 and 9 ka (scenario 1 from Constantinescu
et al., 2015), the 23.8°/C thermal gradients as derived from long-core MeBo measurements
and only differ by the dynamics of sea-bottom temperature warming after reconnection
with the Mediterranean at 9 ka (abrupt near instantaneous change for Case A as proposed
by Erickson and Van Herzen, 1978, more progressive re-equilibrium for Case B as
proposed by Zander et al., 2017).

173

174 **Table *S*1. Different Limit and Boundary Conditions Considered in the Numerical**
175 **Calculations**

176

Modelled Cases	Sea level (Figure S2A)	Sea-bottom temperature variation (Figure S2B)
__Case A__	Constantinescu et al., 2015 – scenario 1 (lowest amplitude sea level variation)	Erickson & Von Herzen, 1978 – scenario 1 (abrupt sea-bottom temperature change at -9 ka)
__Case B__	Constantinescu et al., 2015 – scenario 1 (lowest amplitude sea level variation)	Zander & al., 2017 (progressive sea-bottom temperature change from -9 ka to actual)
__Case C__	Constantinescu et al., 2015 – scenario 1 (lowest amplitude sea level variation)	Erickson & Von Herzen, 1978 – scenario 2 (less-abrupt sea-bottom temperature change at -9 ka)
__Case D__	Constantinescu et al., 2015 – scenario 2 (highest amplitude sea level variation)	Erickson & Von Herzen, 1978 – scenario 1 (abrupt sea-bottom temperature change at -9 ka)
__Case E__	Constantinescu et al., 2015 – scenario 2 (highest amplitude sea level variation)	Erickson & Von Herzen, 1978 – scenario 2 (less-abrupt sea-bottom temperature change at -9 ka)

177

178 **Note.** Inputs are described for each case through different published scenarios or via in-situ measurements,

179 in particularly the scenario of sea-level fluctuations, thermal conditions and sea-bottom temperature

180 evolution presented in Figure S2. Results of all scenarios are shown in Figure S6.

181